Suppressed dependence of polarization on epitaxial strain in highly polar ferroelectrics

Ho Nyung Lee[1], Serge M. Nakhmanson[2], Matthew F. Chisholm[1], Hans M. Christen[1], Karin M. Rabe[2] & David Vanderbilt[2]

[1]*Materials Science and Technology Division, Oak Ridge National Laboratory, Oak Ridge, TN 37831, USA*

[2]*Department of Physics and Astronomy, Rutgers University, Piscataway, NJ 08854-8019, USA*

Epitaxial strain, induced in thin films due to lattice mismatch between the material and the substrate, results in enhanced properties and device performance for many materials. Examples include a higher operation speed and lower power consumption in strain-engineered semiconductor-based devices[1], and a large enhancement of ferroelectric and dielectric responses as well as formation of new phases in certain complex oxide perovskites[2–7]. Although it is tempting to assume that such strong sensitivity to epitaxial strain is common to all perovskite compounds, a recent computational study[8] suggests that this is not universally true. In this work, we present the results of a combined experimental and computational investigation of coupling between polarization and epitaxial strain in the highest-quality ferroelectric $PbZr_{0.2}Ti_{0.8}O_3$ (PZT) thin films grown by pulsed laser deposition onto $SrRuO_3$-electroded $SrTiO_3$ substrates. A comparison of the properties of relaxed (tetragonality $c/a \approx 1.05$) and highly-strained ($c/a \approx 1.09$) films shows that polarization, while being amongst the highest reported for PZT or $PbTiO_3$ in either film or bulk forms ($P_r \approx 82\ \mu C/cm^2$), is almost independent of epitaxial strain. Our first principles calculations support this experimental observation. Furthermore, they show that epitaxial strain induced in materials with already large ferroelectric atomic displacements, such as PZT and $PbTiO_3$, does not have the same strong effect on the polarization as it does in less polar perovskites, for which it can lead to a substantial polarization increase.

In epitaxial ferroelectric films, in-plane biaxial strain leads to a lattice distortion along the normal direction, which often increases their ferroelectric polarization and/or transition temperature[2,3,6,9]. Moreover, room-temperature ferroelectricity can be induced in materials that otherwise would not be ferroelectric[5]. Therefore, epitaxial strain is recognized as a useful tool to influence materials properties. However, the fundamental mechanisms responsible for the coupling between epitaxial strain and ferroelectric polarization in thin films are not yet fully understood, although it is quite clear that they should be manifested most profoundly in coherently grown thin films. In such films misfit dislocation formation is energetically and/or kinetically prohibited and therefore reduction of the polarization by pinning of dipoles by defects is unlikely. However, this is true only for films with thicknesses below a certain critical value (t_c), above which the strain relaxation via defect formation occurs. This thickness depends on the lattice mismatch between the film and the substrate[10,11]: for example, in $BaTiO_3$ on $SrTiO_3$ (in-plane mismatch of 2.4%) a $t_c \approx$ 2-4 nm has been experimentally determined[12,13]. But at such small film thicknesses polarization measurements are hindered by high tunnelling and/or leakage currents[4]. A strong influence of depolarization fields, originating from the incomplete screening of polarization, may also mask the intrinsic effects[14–16]. Therefore, a careful characterization of strain effects is most reliably achieved in a system with a fairly small lattice mismatch with the substrate and, consequently, large t_c (e.g., several 10s of nanometres). Similar considerations have already led to successful

studies of strain effects in $SrTiO_3$ (Ref. 5) and $BaTiO_3$ (Ref. 4). In this work, we grow $PbZr_{0.2}Ti_{0.8}O_3$ films (PZT, $a = b = 0.3953$ nm, $c = 0.4148$ nm, $c/a \approx 1.05$ for an unstrained film)[17] by our well-established pulsed laser deposition (PLD) technique[6], which results in a 1.2 % lattice mismatch with the $SrTiO_3$ substrate (cubic with $a = 0.3905$ nm). For the lattice-matched bottom electrodes on the $SrTiO_3$ substrates, we use atomically-flat, epitaxially-strained $SrRuO_3$ films (thickness ~4 nm)[6,18]. To elucidate the effect of epitaxial strain on the magnitude of polarization, the structural and ferroelectric properties of PZT films are investigated both experimentally and by first-principles calculations. For the latter, other similar perovskite materials, such as $BaTiO_3$ and $PbTiO_3$, also are analyzed for systematic comparison.

The results shown in Fig. 1 demonstrate the structural quality of the current PZT thin films grown on $SrRuO_3$ (4 nm) on (001) $SrTiO_3$ substrate. X-ray diffraction (XRD) θ-2θ scans confirm the *c*-axis orientation of the PZT films without any contribution from *a*-axis oriented domains and impurity phases. $SrRuO_3$ bottom electrodes (same as in Ref. 6) are utilized as templates to grow the PZT films with smooth surfaces, as evidenced by the finite thickness fringes in the XRD scans (Fig. 1b) and the AFM surface topography image (Fig. 1f) with terrace step heights of 0.4 nm, identical to those of the substrate. While only the out-of-plane lattice constant, *c*, is determined by the diffraction peaks in XRD θ-2θ scans, the average in-plane and out-of-plane lattice constants are simultaneously determined by XRD reciprocal space maps (RSMs), with results shown in Figs. 1c and d. The maps confirm that the films grow closely lattice-matched on $SrRuO_3$-electroded $SrTiO_3$ up to about 40 nm in thickness ($a \approx 0.391$ nm, $c/a \approx 1.09$). Above 40 nm PZT thickness, the films relax to a bulk-like state ($a \approx 0.395$ nm, $c/a \approx 1.05$) as seen in Fig. 1e. The sudden decrease of tetragonality in films thicker than ~40 nm suggests that the kinetic barrier for strain relaxation is exceeded at this film thickness. This relatively large critical thickness is attributed to the low growth temperature (625 °C), consistent with the reported behaviour in Ge_xSi_{1-x} (Ref. 11). However, there is still a small but non-negligible drop in the *c*/*a* ratio from 1.095 to 1.087 as the film thickness increases from 15 nm to 40 nm (Fig. 1e). This is related to an increase in the number of dislocations, which do not significantly contribute to the strain relaxation due to their limited number, e.g. the average dislocation spacing seen in a cross section of the 15 nm thick film (Fig. 1g) is ~170 nm. (Note that the dislocation cores are seen not only at the interface, but also a few nanometers above the interface as shown in the inset of Fig. 1g.) A cross section from a relaxed film (116 nm thick), on the other hand, shows a larger number of dislocation lines with an average spacing of ~30 nm (Fig. 1h). This is indeed in a good agreement with the fact that an orthogonal array of dislocations (Burgers vector: **b** = 0.3905 nm) with a spacing of 32 nm would completely relieve the misfit strain.

Figure 2a shows *P(E)* hysteresis loops for two PZT films, with thicknesses of 30 nm (strained) and 100 nm (relaxed). Both films exhibit fully saturated, well-defined square hysteresis loops without any indication of the polarization relaxation. The obtained values for the remnant polarization, $P_r \approx 82$ μC/cm^2 measured at 100 Hz, are amongst the highest reported for PZT and $PbTiO_3$ in film or bulk forms[19]. Pulse measurements of polarization further confirm the absence of any appreciable leakage contribution (switching polarization: $P_{sw} = 162.3$ μC/cm^2 and non-switching polarization: $P_{nsw} = 0.4$ μC/cm^2 even from the 35 nm-thick film as shown in Fig. 2b). The well-defined

switching current curves in the inset of Fig. 2b also indicate that the high values obtained for the polarization are not a consequence of instrumental artefacts or high leakage current.

Since the strained and relaxed films have different defect structure and density (see Figs. 1g and h), in the relaxed case these defects could in principle hinder domain wall motion and thus reduce the switchable polarization, yielding an artificial decrease of polarization with thickness. In contrast, our data reveal almost no difference between the values of polarization in strained and relaxed films: a surprisingly modest polarization enhancement due to strain (Figs. 2c and d), much smaller than the ~ 40% increase expected for $BaTiO_3$ (Ref. 2) or ~ 15% for $PbTiO_3$ (Ref. 20) for similar levels of strain. Such lack of polarization enhancement is quite striking in a material praised for its "strong strain-polarization coupling" and high piezoelectric coefficients[21,22].

In addition to the changes of film tetragonality and polarization (Figs. 2c and d), it is also instructive to analyze the behaviour of the coercive field E_c (i.e., the field required to reverse the polarization) as a function of film thickness. Results extracted from hysteresis loops similar to the ones shown in Fig. 2a are summarized in Fig. 2e. While the values of the coercive fields are significantly larger than those reported for single crystals (10 ~ 100 kV/cm), the dependence follows the Janovec-Kay-Dunn (JKD) scaling law ($E_c(d) \propto d^{-2/3}$)[23,24] over the entire thickness range (20 nm – 200 nm), and is undisturbed by the abrupt change of tetragonality at around 50 nm. We can therefore conclude that the JKD law is insensitive to the presence of bulk defects or the epitaxial-strain state of the films, but may still reflect the changes in switching kinetics related to domain nucleation and growth[25] or depolarization fields[26] with varying film thickness.

To understand the microscopic phenomena behind the observed modest coupling between polarization and epitaxial strain in thin PZT films, we have complemented the experiments with a first principles investigation of atomistic PZT models. The effect of epitaxial strain was isolated by constraining the in-plane lattice parameter a of a bulk crystal to that of a cubic $SrTiO_3$ substrate [the value computed here being 0.3864 nm, a slight underestimate typical of local density approximation (LDA) calculations] and allowing the cell to relax to zero stress in the out-of-plane direction. In the absence of epitaxial strain (i.e. to simulate the relaxed-film environment) the cells were allowed to relax to zero stress in the in-plane direction as well. By averaging over the family of ordered models shown in Fig. 3a, we obtained P = 87.3 μC/cm^2 and c/a = 1.061 for the relaxed PZT, and P = 92.6 μC/cm^2 and c/a = 1.086 for the commensurately strained PZT, which constitutes a 6% polarization increase for an averaged in-plane strain ε = –1%. These results are in excellent agreement with the experimental observations above and confirm the absence of substantial polarization enhancement in PZT due to epitaxial strain.

In order to further understand the fundamental mechanism that can explain the relatively small increase of polarization in PZT, we have calculated the polarization, polarization enhancement (in %), and tetragonality enhancement (in %) with respect to epitaxial strain (shown in Figs. 3b–d, respectively) for tetragonal $BaTiO_3$ and $PbTiO_3$ relaxed to zero stress. Additionally, we have studied a "rescaled $PbTiO_3$" material (r-$PbTiO_3$ in what follows) for which the in-plane lattice constant has been tuned by hand until the tetragonality has the same large value as in the Ti-rich PZT systems. This provides a convenient, easily-computable reference material that mimics many of the properties of the real PZT systems of interest. The in-plane epitaxial strain ε ranged from 0 to –2%, bracketing the present experimental strain of –1.2%. Examination of the figures reveals that all of the aforementioned structures show a similar increase in tetragonality and

polarization: $\Delta c/a \approx$ 5-7% and $P(\varepsilon) - P(0) \approx$ 15-20 μC/cm^2 at $\varepsilon = -2\%$. However, the zero-strain polarization in the lead-based materials is much higher than in $BaTiO_3$, which translates into their much smaller polarization enhancement $\Delta P(\%) = 100 \cdot [P(\varepsilon) - P(0)] / P(0)$.

To understand the nature of the polarization change in even more detail we employed a well known linearized approximation that splits polarization into a set of individual ionic contributions. For the out-of-plane polarization:

$$P \approx \sum_i (\partial P / \partial z_i)^{(0)} \cdot \left(z_i - z_i^{(0)}\right) = V^{-1} \sum_i Z_i^* \cdot \Delta z_i \equiv V^{-1} \sum_i D_i$$

Here Z_i^*, Δz_i and D_i are, respectively, the effective charge tensor component, the displacement from the centrosymmetric position, and the effective dipole moment of ion i in the [001] direction. V is the cell volume and a superscript zero refers to evaluation at centrosymmetric ionic positions corresponding to a nonpolar structure with ferroelectric displacements removed. The values of Z_i^*, Δz_i and D_i for each ion in r-$PbTiO_3$, $PbTiO_3$ and $BaTiO_3$ for epitaxial strains of 0, –1 and –2% are shown in Table 1. The effective charges of the same ionic types for all materials are similar and decrease slightly under applied strain (0-7, 2-10 and 2-20% for r-$PbTiO_3$, $PbTiO_3$ and $BaTiO_3$, respectively, at $\varepsilon = -2\%$), while the ionic out-of-plane displacements in unstrained $BaTiO_3$ are 2-5 times smaller than in $PbTiO_3$ and r-$PbTiO_3$, leading to weaker ionic dipoles and, consequently, total polarization. When the strain is applied ($\varepsilon = -2\%$), however, the ionic displacements in $BaTiO_3$ increase by ~55-85%, while in $PbTiO_3$ they increase by ~25-60% and in r-$PbTiO_3$ by only ~15-30%. Translated into an enhancement of the ionic dipole moments (in %), this results in a much steeper enhancement rate in $BaTiO_3$ than in $PbTiO_3$ or r-$PbTiO_3$ (see Table 1). Very similar

trends for the strain induced changes of Z_i^*, Δz_i and D_i are obtained for the family of PZT models shown in Fig. 3a. Overall, it can be then concluded that since unstrained $PbTiO_3$ and PZT are already very polar and ferroelectric ionic displacements in them are very large, they are rather insensitive to applied epitaxial strain (i.e., these displacements cannot be substantially enlarged by strain). The less polar $BaTiO_3$, on the other hand, is much more sensitive to strain, with the largest changes occurring for the Ba and equatorial oxygen (O_e) ions, which have the smallest out-of-plane displacements in the unstrained configuration (see Table 1).

These observations nicely complement the conclusions of Ref. 8 that connect varying strength of polarization-strain coupling in ferroelectric materials to their different elastic properties. In this investigation we tie this effect to some of the most generic features of perovskite-type structures, namely to the magnitude of ferroelectric ion off-centering in the primitive cell and the relative constancy of ionic effective charges under applied strain.

Therefore, understanding our unexpected experimental observations in the framework of these modeling results illustrates that the term “strong polarization enhancement by epitaxial strain” in thin films cannot be generalized for all ferroelectrics. However, the computational insights at the atomic scale, into the nature of the interplay between polarization and epitaxial strain in perovskite-type ferroelectrics, show that the polar and electromechanical properties could be further manipulated, e.g. by doping or by creating artificially structured materials[2,6,7,27–29]. Consequently, there is a rather well-defined path leading toward developing more efficient non-volatile memories, data storage, and nanoelectromechanical devices.

Methods

Before growing the PZT films, epitaxial $SrRuO_3$ films (4 nm in thickness) were grown by PLD on single-stepped (001) $SrTiO_3$ substrates at 700 °C in 100 mTorr O_2 using a KrF excimer laser (λ = 248 nm). The PZT films were also grown by PLD and are found to be optimally grown at 625 ^oC in 100 mTorr O_2 using a sintered stoichiometric $Pb(Zr_{0.2}Ti_{0.8})O_3$ target, followed by cooling in 50 Torr O_2. The laser repetition rate and laser fluence were kept at 5-10 Hz and 2 J/cm^2, respectively. For the electrical characterization, sputtered Pt top electrodes were patterned by a photolithographic lift-off process, yielding pads 100 μm in diameter. Ferroelectric hysteresis loops were recorded by a TF tester (aixACCT Systems) at 100 Hz. Pulse measurements [positive up negative down (PUND)] were performed at 0.0025 s of write/read-pulse time with one second write-pulse delay.

To reflect as faithfully as possible the disordered nature of the $PbZr_{0.2}Ti_{0.8}O_3$ solid solution, given computational constraints, we constructed a family of smaller ordered supercells with varying arrangements of Zr and Ti atoms and then averaged the results of our calculations over this family. Moreover, since the experimental 20/80 Zr-to-Ti concentration ratio is difficult to reproduce in a compact unit cell, it was changed to a more accommodating 25/75 ratio as shown in Fig. 3a. All the calculations presented here were performed under periodic boundary conditions. A plane-wave based density-functional theory (DFT) LDA method [VASP (http://cms.mpi.univie.ac.at/vasp/)] was utilized for the ionic relaxation of the models. The calculations were performed with a plane-wave energy cutoff of 500 eV. During the relaxation the symmetry in all the models was restricted to space group *P*4*mm* (point group C_{4v}). The system was considered to be at equilibrium when the Hellman-Feynman forces on the ions were less than 0.5×10^{-2} eV/Å and the appropriate stress-tensor components smaller than 0.2 Kbar. A 4×4×4 Monkhorst-Pack (MP) mesh was used for all the Brillouin-zone integrations.

We employed the Berry-phase method of the modern polarization theory[30] to compute the total polarization of each model. The 4×4×8 MP mesh used in the polarization calculations produced well-converged results. Another DFT-LDA method [PWscf (www.pwscf.org)] was used to compute the ionic effective charges in the relaxed models.

References

1. Ieong, M., Doris, B., Kedzierski, J., Rim, K. & Yang, M. Silicon device scaling to the sub-10-nm regime, *Science* **306**, 2057–2060 (2004).
2. Neaton, J. B. & Rabe, K. M. Theory of polarization enhancement in epitaxial $BaTiO_3/SrTiO_3$ superlattices. *Appl. Phys. Lett*. **82**, 1586–1588 (2003).
3. Wang, J. *et al*. Epitaxial $BiFeO_3$ multiferroic thin film heterostructures, *Science* **299**, 1719–1722 (2003).
4. Choi, K. J. *et al*. Enhancement of ferroelectricity in strained $BaTiO_3$ thin films, *Science* **306**, 1005–1009 (2004).
5. Haeni, J. H. *et al*. Room-temperature ferroelectricity in strained $SrTiO_3$, *Nature* **403**, 758–761 (2004).
6. Lee, H. N., Christen, H. M., Chisholm, M. F., Rouleau, C. M. & Lowndes, D. H. Strong polarization enhancement in asymmetric three-component ferroelectric superlattices, *Nature* **433**, 395–399 (2005).
7. Nakhmanson, S. M., Rabe, K. M. & Vanderbilt, D. Predicting polarization enhancement in multicomponent ferroelectric superlattices, *Phys. Rev. B* **73**, 060101(R) (2006).
8. Ederer, C. & Spaldin, N. Effect of epitaxial strain on the spontaneous polarization of thin film ferroelectrics, *Phys. Rev. Lett*. **95**, 257601 (2005).
9. Pertsev, N. A., Zembilgotov, A. G. & Tagantsev, A. K. Effect of mechanical boundary conditions on phase diagrams of epitaxial ferroelectric thin films, *Phys. Rev. Lett*. **80**, 1988–1991 (1998).
10. Matthews, J. W. & Blakeslee, A. E. Defects in epitaxial multilayers: I. Misfit dislocations, *J. Cryst. Growth* **27**, 118–125 (1974).

11. People, R. & Bean, J. C. Calculation of critical layer thickness versus lattice mismatch for Ge_xSi_{1-x}/Si strained-layer heterostructures, *Appl. Phys. Lett*. **47**, 322–324 (1985).
12. Sun, H. P., Tian, W., Pan, X. Q. Haeni, J. H. & Schlom, D. G. Evolution of dislocation arrays in epitaxial $BaTiO_3$ thin films grown on (100) $SrTiO_3$, *Appl. Phys. Lett*. **84**, 3298–3330 (2004).
13. He, J. Q., Vasco, E. Dittmann, R. & Wang, R. H. Growth dynamics and strain relaxation mechanisms in $BaTiO_3$ pulsed laser deposited on $SrRuO_3/SrTiO_3$, *Phys. Rev. B* **73** 125413 (2006).
14. Junquera, J. & Ghosez, P. Critical thickness for ferroelectricity in perovskite ultrathin films, *Nature*, **422**, 506–509 (2003).
15. Lichtensteiger, C., Triscone, J.-M., Junquera, J. & Ghosez, P. Ferroelectricity and tetragonality in ultrathin $PbTiO_3$ Films, *Phys. Rev. Lett*. **94**, 047603 (2005).
16. Kim, D. J. *et al*. Polarization relaxation induced by a depolarization field in ultrathin ferroelectric $BaTiO_3$ capacitors, *Phys. Rev. Lett*. **95**, 237602 (2005).
17. Frantti, J. *et al.* Neutron diffraction studies of $Pb(Zr_xTi_{1-x})O_3$ ceramics, *Jpn. J. Appl. Phys*. **39**, 5697–5703 (2000).
18. Hong, W. *et al*. Persistent step-flow growth of strained films on vicinal substrates, *Phys. Rev. Lett.* **95**, 095501 (2005).
19. Hellwege, K.-H. & Hellwege, A. M. Landolt-Börnstein: Numerical Data and Functional Relationships in Science and Technology, New Series, Group III, Vol. 16. (Springer-Verlag, Berlin, 1981).
20. Bungaro, C. & Rabe, K. M. Epitaxially strained $[001]-(PbTiO_3)_1(PbZrO_3)_1$ superlattice and $PbTiO_3$ from first principles, *Phys. Rev. B* **69**, 184101 (2004).

21. Cohen, R. E. Origin of ferroelectricity in perovskite oxides, *Nature* **358**, 136–138 (1992).

22. Rabe, K. M. & Waghmare, U. V. Strain coupling in the $PbTiO_3$ ferroelectric transition, *Phil. Trans. R. Soc. Lond. A* **354**, 2897–2914 (1996).

23. Janovec, V. On the theory of the coercive field of single-domain crystals of $BaTiO_3$, *Czech. J. Phys*. **8**, 3–15 (1958).

24. Kay, H. F. & Dunn, J. W. Thickness dependence of the nucleation field of triglycine sulphate, *Phil. Mag.* **7**, 2027–2034 (1962).

25. Scott, J. F. Ferroelectric Memories (Springer, Berlin, 2000).

26. Dawber, M., Chandra, P., Littlewood, P. B., & Scott, J. F. Depolarization corrections to the coercive field in thin-film ferroelectrics, *J. Phys.: Condens. Matter* **15**, L393–L398 (2003).

27. George, A. M., Íñiguez, J. & Bellaiche, L. Anomalous properties in ferroelectrics induced by atomic ordering, *Nature* **413**, 54–57 (2001).

28. Grinberg, I., Cooper, V. R. & Rappe, A. M. Relationship between local structure and phase transitions of a disordered solid solution, *Nature* **419**, 909–911 (2002).

29. Ghita, M., Fornari, M., Singh, D. J. & Halilov, S. V. Interplay between *A*-site and *B*-site driven instabilities in perovskites, Phys. Rev. B **72**, 054114 (2005).

30. King-Smith, R. D. & Vanderbilt, D. Theory of polarization of crystalline solids, *Phys. Rev. B* **47**, 1651–1654 (1993).

Acknowledgements The authors thank Douglas H. Lowndes for careful reading and valuable comments. Research sponsored by the Division of Materials Sciences and Engineering, Office of Basic Energy Sciences, U.S. Department of Energy, under contract DE-AC05-00OR22725 with Oak Ridge National Laboratory, managed and

operated by UT-Battelle, LLC and by the Center for Piezoelectrics by Design (CPD) under ONR Grant N00014-01-1-0365. The calculations were done at MHPCC DoD supercomputing center.

Author Contributions H.N.L. performed the PLD synthesis and characterization as well as the integration of experimental and computational components. S.M.N., K.M.R. and D.V. were responsible for the computations and their analysis. M.F.C. conducted the Z-contrast STEM work. H.M.C. assisted with the experimental components. All authors discussed the results and commented on the manuscript.

Author Information Reprints and permissions information is available at npg.nature.com/reprintsandpermissions. The authors declare no competing financial interests. Correspondence and requests for materials should be addressed to H.N.L. (hnlee@ornl.gov).

Figure captions

Figure 1 Structural quality and lattice constants of PZT films grown on $SrRuO_3/SrTiO_3$. **a**, XRD θ–2θ scan of a 20 nm-thick PZT film revealing the pure *c*-axis orientation. **b**. XRD θ–2θ scans around the 001 reflection of 20, 50, and 100 nm thick films, clearly showing the increase of out-of-plane lattice constant by reducing the film thickness. The peak broadening, especially from the 20 nm thick film, is due to the finite film thickness while the fringes originate from the high quality surface and interface of the film. Note that the reflection from $SrRuO_3$ is not appreciable due to a rather small thickness (4 nm). **c**,**d**, XRD-RSMs (Q_{110} and Q_{001} are reciprocal in-plane and out-of-plane lattice constants in units of 1/*d*) recorded around the 114 peak of (**c**) 30 and (**d**) 100 nm thick PZT films, indicating clearly the different strain states of the two films. The dotted red and blue lines mark the 114 $SrTiO_3$ peak position and that of PZT, respectively. **e**, In-plane and out-of-plane lattice constants as a function of film thickness. **f**, AFM topographic image (image size: $6 \times 8\ \mu m^2$) with single terrace steps (~0.4 nm) of an atomically-flat PZT film (40 nm in thickness). The terrace steps are mimicked from the $SrTiO_3$ substrate, nicely transferring the high crystallinity of the substrate through the $SrRuO_3$ bottom electrode layer. **g**,**h**, Cross-sectional Z-contrast images of (**g**) 15 and (**h**) 116 nm thick PZT films. The inset of **g** is a high-resolution image of the 15 nm thick film showing a dislocation core located 6 nm above the $SrRuO_3$ layer. The arrows in yellow in **g** and **h** point to the dislocation lines, clearly indicating the reduced dislocation density in the well-strained film. STO and SRO stand for $SrTiO_3$ and $SrRuO_3$.

Figure 2 Thickness dependence of tetragonality, ferroelectric polarization and coercive field. **a**, P(E) hysteresis loops at 100 Hz from 35 and 100 nm thick PZT films. **b**, Simultaneously-measured pulse polarization and switching current

(inset) by applying trapezoid pulses (P1 to P4), showing neither non-switching current nor non-switching polarization. **c**,**d**,**e**, Tetragonality (**c**), remanent polarization (**d**) and coercive field (**e**) as a function of film thickness. The additional epitaxial strain does not change the polarization, while the slope (–0.614±0.067) in the inset of **e** is in good agreement with the classical scaling behaviour ($E_c \propto d^{-2/3}$).

Figure 3 Structural parameters and polarization in r-$PbTiO_3$, $PbTiO_3$ and $BaTiO_3$ under varying degrees of epitaxial strain ε from the first-principles calculations. **a**, Three ordered models for $PbZr_{0.25}Ti_{0.75}O_3$ used in the calculations. **b**,**c**,**d**, Polarization (**b**), polarization enhancement (**c**) and tetragonality enhancement (**d**) in $BaTiO_3$, $PbTiO_3$ and r-$PbTiO_3$ are shown as a function of epitaxial strain ε.

Table 1: Strain-induced changes of Δz, Z* and D.

System	Atom	ε = 0%			ε = –1%			ε = –2%		
		Δz (Å)	Z^*	D (D)	Δz (Å)	Z^*	D (D)	Δz (Å)	Z^*	D (D)
r-$PbTiO_3$	Pb	0.364	3.313	5.799	0.370	3.334	5.924	0.411	3.305	6.525
	Ti	0.160	5.273	4.044	0.179	5.158	4.443	0.213	4.979	5.088
	O_e	-0.177	-2.069	1.755	-0.185	-2.085	1.850	-0.203	-2.067	2.019
	O_a	-0.142	-4.493	3.064	-0.150	-4.368	3.156	-0.187	-4.200	3.769
$PbTiO_3$	Pb	0.286	3.485	4.795	0.301	3.478	5.023	0.355	3.409	5.812
	Ti	0.140	5.520	3.720	0.166	5.298	4.221	0.209	5.058	5.081
	O_e	-0.153	-2.198	1.619	-0.166	-2.191	1.746	-0.193	-2.158	1.997
	O_a	-0.092	-4.650	2.047	-0.106	-4.439	2.260	-0.149	-4.202	3.006
$BaTiO_3$	Ba	0.033	2.795	0.442	0.044	2.813	0.601	0.057	2.842	0.783
	Ti	0.082	6.235	2.466	0.107	5.673	2.904	0.128	5.218	3.229
	O_e	-0.020	-2.023	0.191	-0.029	-1.968	0.271	-0.037	-1.923	0.338
	O_a	-0.048	-5.022	1.159	-0.065	-4.600	1.444	-0.084	-4.262	1.727

Ferroelectric displacements Δz, effective charges Z^* and associated dipole moments D of individual ions in tetragonal r-$PbTiO_3$, $PbTiO_3$ and $BaTiO_3$ under varying degrees of epitaxial strain ε are listed. For the same strain applied, ionic dipole moments in $BaTiO_3$, although being smaller than those in $PbTiO_3$, grow at a faster rate, which results in a higher degree of polarization enhancement. Equatorial oxygens O_e are at positions (½,0, ½) and (0, ½,½), and apical oxygen O_a is at position (½,½,0) in the crystalline coordinate system.

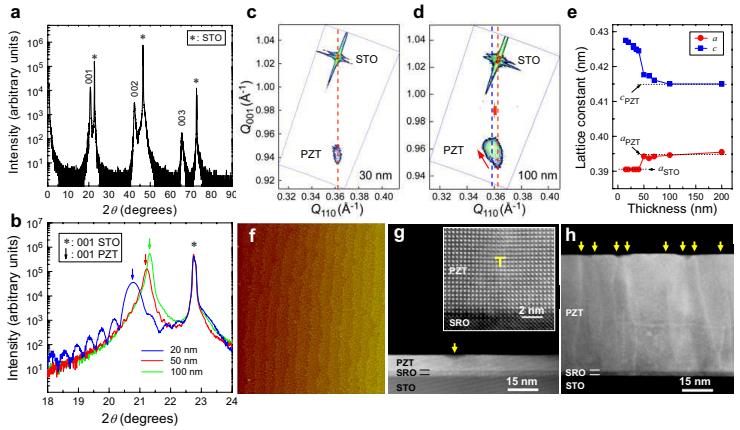

Fig. 1. H. N. Lee *et al.*

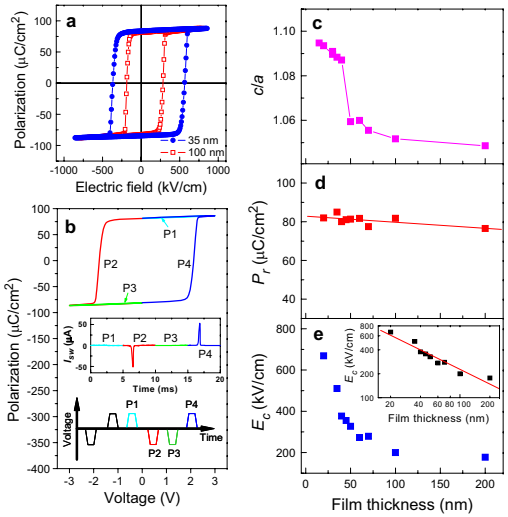

Fig. 2. H. N. Lee *et al.*

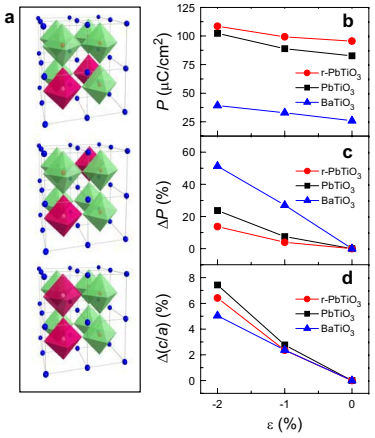

Fig. 3. H. N. Lee *et al.*